CHALMERS
UNIVERSITY OF TECHNOLOGY

Transformational cloaking from seismic surface waves by micropolar metamaterials with finite couple stiffness

Wave Motion 58 (2015) 53–67

Contents lists available at ScienceDirect

Wave Motion

journal homepage: www.elsevier.com/locate/wavemoti

Transformational cloaking from seismic surface waves by micropolar metamaterials with finite couple stiffness

Alexey Khlopotin, Peter Olsson *, Fredrik Larsson

Chalmers University of Technology, Department of Applied Mechanics, SE-412 96 Gothenburg, Sweden

HIGHLIGHTS

- We have studied the possibilities for cloaking of structures using transformational elastodynamics.
- An almost perfect cloak is obtained by letting the size of the structure tend to zero in the fictitious domain.
- Two models for elastodynamic cloaking are considered; the restricted and the unrestricted micropolar medium.
- The more physical unrestricted micropolar medium approaches the restricted case for high couple stiffness.
- The possibility to cloak a cylinder in 2D has been shown, limited by the coefficients in the unrestricted micropolar medium, in numerical simulations.

ARTICLE INFO

Article history:
Received 24 November 2014
Received in revised form 16 June 2015
Accepted 2 July 2015
Available online 8 July 2015

Keywords:
Cloaking
Metamaterials
Micropolar continuum
Transformational elastodynamics
Seismic waves

ABSTRACT

Transformational elastodynamics can be used to protect sensitive structures from harmful waves and vibrations. By designing the material properties in a region around the sensitive structure, a cloak, the incident waves can be redirected as to cause minimal or no harmful response on the pertinent structure. In this paper, we consider such transformational cloaking built up by a suitably designed metamaterial exhibiting micropolar properties. First, a theoretically perfect cloak is obtained by designing the properties of an (unphysical) restricted micropolar material within the surrounding medium. Secondly, we investigate the performance of the cloak under more feasible design criteria, relating to finite elastic parameters. In particular, the behavior of a physically realizable cloak built up by unrestricted micropolar elastic media is investigated. Numerical studies are conducted for the case of buried as well as surface breaking structures in 2D subjected to incident Rayleigh waves pertinent to seismic loading. The studies show how the developed cloaking procedure can be utilized to substantially reduce the response of the structure. In particular, the results indicate the performance of the cloak in relation to constraints on the elastic parameters.

1. Introduction

Ancient civilizations discovered that by arranging the interface between important structures, *e.g.* temples, and the underlying ground, it is possible to achieve some protection against seismic waves, that might otherwise damage the structures. Pliny the Elder describes a successful protective strategy, involving erecting the buildings on foundations with layers of "sheepskins with their flecees unshorn" and carbon gravel [1]. With this arrangement the buildings could survive many earthquakes with comparatively little damage, by essentially allowing the ground to slip and slide beneath the buildings.

* Corresponding author. Tel.: +46 317723725.
E-mail addresses: alexey.khlopotin@chalmers.se (A. Khlopotin), peter.olsson@chalmers.se (P. Olsson), fredrik.larsson@chalmers.se (F. Larsson).

http://dx.doi.org/10.1016/j.wavemoti.2015.07.002

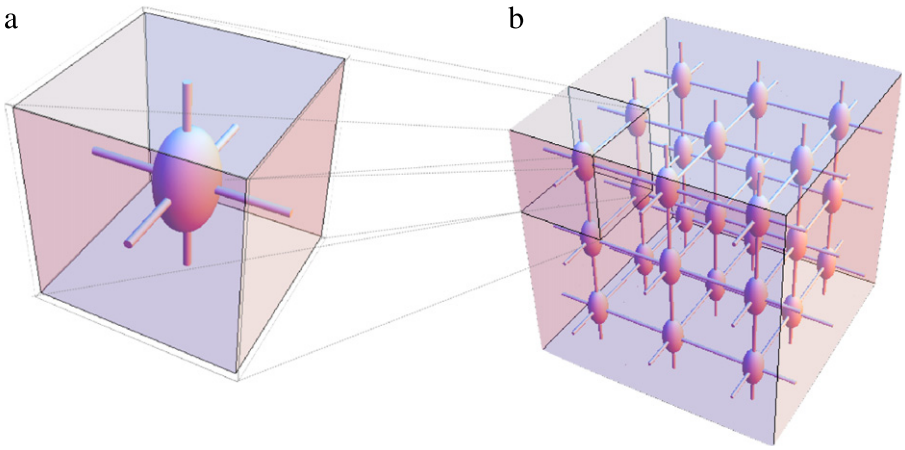

Fig. 1. Schematic sketches of the assumed microstructure of a micropolar material. (a) A typical representative volume element (RVE) on the microscale. A body attached to a connective fabric is embedded in an elastic material. The embedded central body contributes to the microscale moment of inertia tensor, as well as to the macro scale local density. The connective fabric contributes to the microscale couple stiffness tensor. (b) A small part of the micropolar material consisting of a multitude of connected RVEs. Note that a homogenized continuum model is used for the material and no calculations are performed on the microstructural level.

A considerably more modern method to control seismic waves is the use of so-called sonic, or phononic, crystals. The idea is to utilize in an intelligent manner the passband/stopband properties of periodic structures. [2] describes a recent large scale experimental investigation of this type of approach to seismic protection.

Roughly a decade ago, another possible route to earthquake protection was suggested, also relying on the construction of a carefully designed foundation. It started with the discovery of transformational cloaking, initially for electric impedance tomography, by Greenleaf, Lassas, and Uhlmann [3]. Soon to follow were extensions of the approach to electrodynamics [4], elastodynamics [5] and acoustics [6]. By now there is an extensive body of work on elastodynamic and acoustic cloaking. Many approaches, including active cloaking [7,8], as well as the use of pre-stress [9–11], have been proposed. An approximate standard model for cloaking is given in [12].

Early on, it was suggested that cloaking could be utilized to protect structures against seismic surface waves [13], by placing a suitable cloaking layer around the structure to be protected. To put the protecting layer on the surface, rather than bury it beneath, may be motivated by the fact that at least at some distance from the epicenter of the seismic event causing the seismic waves, the harmful waves are to a large extent surface waves, so-called Rayleigh waves, rather than bulk waves. The dominance of surface waves is due to the geometric attenuation in 2D being slower than that in 3D. The type of surface wave cloak described in [13] is an idealized plate, satisfying a wave equation that might be non-trivial to realize in practice. Other cloak models for plates may be found in the literature, *e.g.*, in [14,15].

A perhaps more realistic approach to Rayleigh wave cloaking is to take advantage of the fact that a graded restricted micropolar material may be utilized for cloaking, as described in [16] and generalized in [17]. For a description of the theory of micropolar continua, see, *e.g.*, [18,19]. The presumed microstructure of a micropolar material is sketched in Fig. 1. Note that the figure is only for illustration purposes as a homogenized continuum model is used in this paper. 'Restricted' here indicates that the micropolar material is assumed to have infinite micro stiffness, essentially locking the micro rotation to a constant value, typically zero. As this type of cloak in theory works for any kind of linear elastic bulk wave, it should work also for a Rayleigh surface wave, as this may be considered as a certain superposition of vertically attenuated P and S waves. In the present paper this is verified and checked numerically, using the commercial software COMSOL Multiphysics™.

The practical feasibility of utilizing graded micropolarity for elastodynamic cloaking, hinges to a great extent on how well the condition of infinite micro stiffness (a.k.a. couple stiffness) may be approximated. The problem of infinities required in various cloaking scenarios has been pointed out repeatedly, *cf. e.g.* [6]. But in practice, the infinite may of course often be supplanted by the very large. A case in point is partial cloaking by graded fiber-reinforced composites, where the inextensibility of the fibers may be replaced by a very large stiffness along the fiber direction as compared to the stiffness perpendicular to the fibers [20]. Similarly, it is of interest to see how well a micropolar cloak with high couple stiffness can approximate the (potentially perfect) restricted micropolar cloak. There is also the possibility of mapping the hidden object not to a point (or line) but to a small sphere (or cylinder) so as to avoid infinities due to singular points of the mapping. While this again would make the cloak less than perfect, this drawback might be offset by making it possible to actually manufacture. Similar suggestions for partial cloaking may be found in the literature: in [21], it was proposed to map a ball of small, but finite, radius to the inner boundary, and in [6] and [22] regularization was applied.

Another question, also related to the potential real-world performance of a micropolar cloak, is the extent to which the actual size of the microscale affects the performance of the cloak. While this is of course a matter that properly should be investigated experimentally, it is here suggested that it is possible to get some information on this scale dependence directly from the finite element analysis of the cloak. Contrary to most other contexts, where mesh dependence effects are

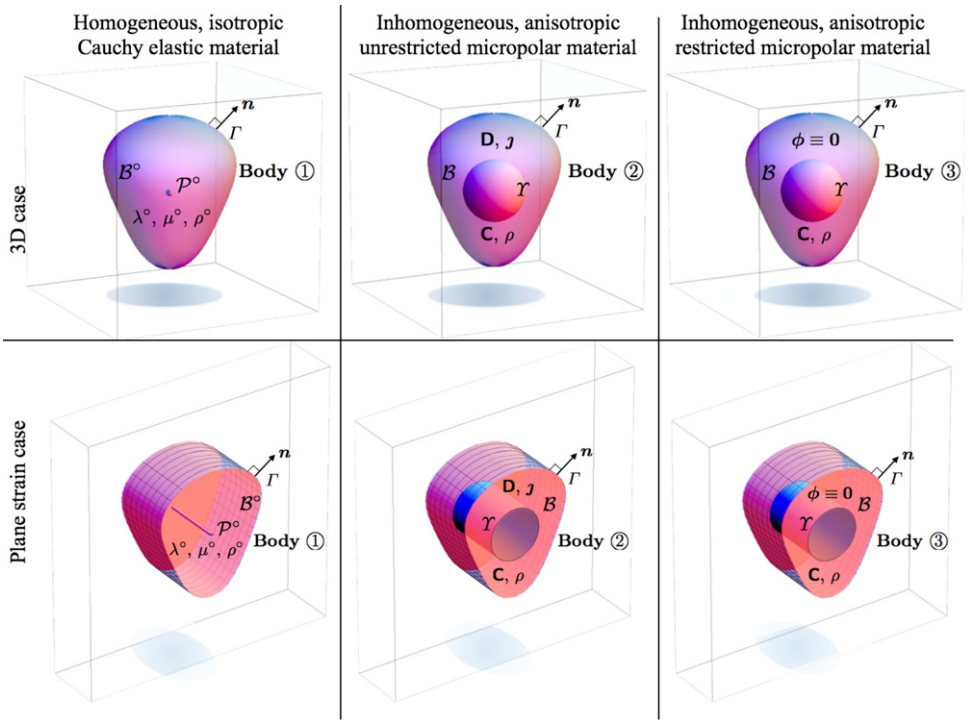

Fig. 2. The three types of bodies occupying the region $\mathcal{B}^\circ$ or the region $\mathcal{B}$, respectively: **Body** ① with homogeneous isotropic elastic Cauchy material (Lamé parameters λ°, μ°, and mass density ρ°); **Body** ② with anisotropic, inhomogeneous (unrestricted) micropolar medium (stiffness tensor $\mathbf{C} = \mathbf{C}(\boldsymbol{x})$, couple stiffness tensor $\mathbf{D} = \mathbf{D}(\boldsymbol{x})$, moment of inertia density tensor $\boldsymbol{J}$, and mass density $\rho = \rho(\boldsymbol{x})$); **Body** ③ with restricted micropolar medium. Upper row: 3D case, with $\mathcal{P}^\circ$ being a point. Lower row: Plane strain case, with $\mathcal{P}^\circ$ being a line perpendicular to the plane of displacements.

undesirable, the mesh dependence of the solution to the Rayleigh wave scattering problem considered in this paper carries important design information.

As mentioned above, the importance of boundary conditions was recognized early in the history of seismic protection schemes. In this paper we consider the importance of the boundary conditions for the effectiveness of the (restricted and general) micropolar cloaks against Rayleigh waves. In particular we analyze the inner boundary conditions between the cloaked structure and the cloaking layer.

It could be argued that any cloaking type seismic protection would be far to costly to implement, thus making the considerations of the present paper a very 'academic' exercise. While it is no doubt true that any such cloak will be costly, the cost should of course be weighted against the possible benefits from its use. At present, there are well over four hundred nuclear power plants being operated worldwide. The number is increasing steadily, with roughly sixty plants presently under construction in more than a dozen countries. Many existing and planned nuclear power stations are in or near earthquake zones, and a nuclear plant is often supposed to have a life time in excess of a century. The risk of a seismic event causing a major nuclear disaster, with enormous ensuing human and financial costs, is therefore probably not negligible. The cost of constructing cloaking foundations when new nuclear power plants are built might be motivated in this manner. The time seems ripe for serious consideration of this approach to seismic protection.

2. The cloaking transformation and two kinds of micropolar continua

2.1. Preliminaries

Elastodynamic transformational cloaking theory, of the type introduced by Brun et al. [16], essentially in the systematic form given by Norris and Shuvalov [17] is described in the present section. It is assumed that all deformations and deformation gradients are in the linear regime. We consider three different settings as specified in Fig. 2. The first body, Body ①, is a homogeneous, isotropic Cauchy elastic solid, with a point $\mathcal{P}^\circ$ removed. The second, Body ②, is an inhomogeneous, anisotropic *'unrestricted' micropolar* elastic solid, with a ball of radius r_0 removed. Here we use 'unrestricted' to denote that no couple stiffness nor rotational inertia of the microstructure of the micropolar material is set to infinity, and no 'hand of god' type of constraint is imposed on the micropolar microstructure. The third body, Body ③, is an inhomogeneous, anisotropic *restricted micropolar* elastic solid, with a ball of radius r_0 removed. The restricted micropolar body has infinite couple stiffness tensor, and/or infinite micro moment of inertia tensor.

The homogeneous Cauchy elastic body (the quantities related to which are denoted by a superscript circle "∘"), and the two inhomogeneous micropolar continua are assumed to have identical outer boundaries, Γ. All the bodies thus have a boundary consisting of two disjoint connected components; an outer, Γ, and an inner boundary, $\{\mathcal{P}^\circ\}$ or Υ, respectively.

Below, we describe in detail the properties of these three bodies. To roughly indicate what we mean by 'restricted' and 'unrestricted' micropolar continuum, we may say that in the unrestricted micropolar medium, the stiffness tensor, the mass density *and* the couple stiffness tensor and the inertia tensor are all finite.

While the situation to be addressed in later sections is that where the bodies are (partially or completely) embedded in a surrounding homogeneous material and waves are scattered from the bodies, initially only a boundary value problem is considered.

Thus assume that the same prescribed traction vector field $\boldsymbol{g}$ is applied to Γ for all three bodies. For the **homogeneous body**, **Body** ①, the boundary value problem is

$$\text{Equation of motion}: \quad \nabla^\circ \bullet \boldsymbol{\sigma}^\circ(\boldsymbol{x}^\circ, t) = \rho^\circ\, \partial_t^2 \boldsymbol{u}^\circ(\boldsymbol{x}^\circ, t), \qquad (\boldsymbol{x}^\circ, t) \in \mathcal{B}^\circ \times [0, T]. \tag{1a}$$

$$\text{Constitutive relation}: \quad \boldsymbol{\sigma}^\circ(\boldsymbol{x}^\circ, t) = \mathbf{C}^\circ \vdots [\nabla^\circ \otimes \boldsymbol{u}^\circ(\boldsymbol{x}^\circ, t)]^{\mathrm{t}}, \qquad (\boldsymbol{x}^\circ, t) \in \mathcal{B}^\circ \times [0, T]. \tag{1b}$$

$$\text{Initial conditions}: \quad \boldsymbol{u}^\circ(\boldsymbol{x}^\circ, 0^+) = \mathbf{0} \quad \text{and} \quad \partial_t \boldsymbol{u}^\circ(\boldsymbol{x}^\circ, 0^+) = \mathbf{0}, \quad \boldsymbol{x}^\circ \in \mathcal{B}^\circ. \tag{1c}$$

$$\text{Outer boundary condition}: \quad (\boldsymbol{\sigma}^\circ \bullet \boldsymbol{n})|_\Gamma = \boldsymbol{g}(\boldsymbol{x}^\circ, t), \qquad (\boldsymbol{x}^\circ, t) \in \Gamma \times [0, T]. \tag{1d}$$

$$\text{Inner boundary condition}: \quad \textit{To be specified}. \text{ (See below.)} \qquad \boldsymbol{x}^\circ \to \mathcal{P}^\circ, \ t \in [0, T]. \tag{1e}$$

The double contraction, denoted by "$\vdots$", is here defined so that, *e.g.*,

$$\boldsymbol{R} \vdots \boldsymbol{S} = R_{ij} S_{ij} \quad \text{for } \boldsymbol{R} = R_{ij}\, \mathbf{e}_i \otimes \mathbf{e}_j \text{ and } \boldsymbol{S} = S_{ij}\, \mathbf{e}_i \otimes \mathbf{e}_j,$$

$$\boldsymbol{R} \vdots \mathbf{P} = R_{ij} P_{ijk\ell}\, \mathbf{e}_k \otimes \mathbf{e}_\ell \quad \text{for } \boldsymbol{R} = R_{ij}\, \mathbf{e}_i \otimes \mathbf{e}_j \text{ and } \mathbf{P} = P_{ijk\ell}\, \mathbf{e}_i \otimes \mathbf{e}_j \otimes \mathbf{e}_k \otimes \mathbf{e}_\ell.$$

$\boldsymbol{u}^\circ$ is the displacement vector field, while $\boldsymbol{\sigma}^\circ$ is the stress tensor field. The vector field $\boldsymbol{n}$ is the outward pointing unit normal field of Γ. $\boldsymbol{g}(\boldsymbol{x}^\circ, t)$ is the prescribed traction vector field on Γ. For **Body** ①, the fourth order tensor $\mathbf{C}^\circ$ is required to be both minor symmetric and major symmetric, *cf.* below. Several types of transposition are used here and in the following. One is the 'minor' transposition of second order tensors, used above in Eq. (1b), *etc.*, denoted by superscript "t":

$$\boldsymbol{R}^{\mathrm{t}} = R_{ij}\, \mathbf{e}_j \otimes \mathbf{e}_i \quad \text{for } \boldsymbol{R} = R_{ij}\, \mathbf{e}_i \otimes \mathbf{e}_j.$$

(In Eq. (2), this transposition is *distributed to the individual second order tensor elements*, and it is *not* a transposition of the block matrix or block vector.)

A typical boundary value problem for the **unrestricted micropolar body**, **Body** ②, is

$$\text{Equation of motion}: \quad \begin{pmatrix} \mathbf{I} \otimes \nabla & 0 \\ -\boldsymbol{\epsilon} & \mathbf{I} \otimes \nabla \end{pmatrix} \vdots \begin{pmatrix} \boldsymbol{\sigma}(\boldsymbol{x}, t) \\ \boldsymbol{\mu}(\boldsymbol{x}, t) \end{pmatrix}$$

$$= \begin{pmatrix} \mathbf{I}\rho(\boldsymbol{x})\, \partial_t^2 & 0 \\ 0 & \boldsymbol{\jmath}(\boldsymbol{x}) \partial_t^2 \end{pmatrix} \bullet \begin{pmatrix} \boldsymbol{u}(\boldsymbol{x}, t) \\ \boldsymbol{\phi}(\boldsymbol{x}, t) \end{pmatrix}, \quad (\boldsymbol{x}, t) \in \mathcal{B} \times [0, T]. \tag{2a}$$

$$\text{Constitutive relation}: \quad \begin{pmatrix} \boldsymbol{\sigma}(\boldsymbol{x}, t) \\ \boldsymbol{\mu}(\boldsymbol{x}, t) \end{pmatrix}$$

$$= \begin{pmatrix} \mathbf{C}(\boldsymbol{x}) & 0 \\ 0 & \mathbf{D}(\boldsymbol{x}) \end{pmatrix} \vdots \left[\begin{pmatrix} \nabla \otimes \mathbf{I} & -\boldsymbol{\epsilon} \\ 0 & \nabla \otimes \mathbf{I} \end{pmatrix} \bullet \begin{pmatrix} \boldsymbol{u}(\boldsymbol{x}, t) \\ \boldsymbol{\phi}(\boldsymbol{x}, t) \end{pmatrix} \right]^{\mathrm{t}}, \quad (\boldsymbol{x}, t) \in \mathcal{B} \times [0, T]. \tag{2b}$$

$$\text{Initial conditions}: \quad \left. \begin{pmatrix} \boldsymbol{u} \\ \boldsymbol{\phi} \end{pmatrix} \right|_{t=0^+} = \begin{pmatrix} \mathbf{0} \\ \mathbf{0} \end{pmatrix} \quad \text{and} \quad \left. \begin{pmatrix} \partial_t \boldsymbol{u} \\ \partial_t \boldsymbol{\phi} \end{pmatrix} \right|_{t=0^+} = \begin{pmatrix} \mathbf{0} \\ \mathbf{0} \end{pmatrix}, \quad \boldsymbol{x} \in \mathcal{B}. \tag{2c}$$

$$\text{Outer boundary condition}: \quad (\boldsymbol{\sigma} \bullet \boldsymbol{n})|_\Gamma = \boldsymbol{g}(\boldsymbol{x}, t) \quad \text{and} \quad (\boldsymbol{\mu} \bullet \boldsymbol{n})|_\Gamma = \mathbf{0}, \quad (\boldsymbol{x}, t) \in \Gamma \times [0, T]. \tag{2d}$$

$$\text{Inner boundary condition}: \quad \textit{To be specified}. \ (\textit{See below}.) \quad \boldsymbol{x} \in \Upsilon, \ t \in [0, T]. \tag{2e}$$

Note that the couple traction $\boldsymbol{\mu} \bullet \boldsymbol{n}$ isassumed to vanish on the outer boundary; the endpoints of the microstructure network have free ends at Γ. $\boldsymbol{\epsilon}$ is the completely antisymmetric (third-order) Levi-Civita tensor.

For **Body** ②, neither the fourth order tensor $\mathbf{C}$, nor $\mathbf{D}$, is required to be minor symmetric. However, both are major symmetric; *cf.* below.

A typical boundary value problem for the **restricted micropolar body**, **Body** ③, is obtained by forcing $\boldsymbol{\phi} \equiv \mathbf{0}$. The boundary value problem for **Body** ③ is thus which closely resembles the problem for the **Body** ①:

$$\text{Equation of motion}: \quad \nabla \bullet \boldsymbol{\sigma}(\boldsymbol{x}, t) = \rho\, \partial_t^2 \boldsymbol{u}(\boldsymbol{x}, t), \qquad (\boldsymbol{x}, t) \in \mathcal{B} \times [0, T]. \tag{3a}$$

$$\text{Constitutive relation}: \quad \boldsymbol{\sigma}(\boldsymbol{x}, t) = \mathbf{C} \vdots [\nabla \otimes \boldsymbol{u}(\boldsymbol{x}, t)]^{\mathrm{t}}, \qquad (\boldsymbol{x}, t) \in \mathcal{B} \times [0, T]. \tag{3b}$$

$$\text{Initial conditions}: \ \boldsymbol{u}(\boldsymbol{x}, 0^+) = \boldsymbol{0} \quad \text{and} \quad \partial_t \boldsymbol{u}(\boldsymbol{x}, 0^+) = \boldsymbol{0}, \quad \boldsymbol{x} \in \mathcal{B}. \tag{3c}$$

$$\text{Outer boundary condition}: \ (\boldsymbol{\sigma} \bullet \boldsymbol{n})|_{\Gamma} = \boldsymbol{g}(\boldsymbol{x}, t), \qquad (\boldsymbol{x}, t) \in \Gamma \times [0, T]. \tag{3d}$$

$$\text{Inner boundary condition}: \ \textit{To be specified.} \ (\text{See below.}) \quad \boldsymbol{x} \in \Upsilon, \ t \in [0, T]. \tag{3e}$$

A few other types of transposition which we will have occasion to utilize in the following are these: Transposition of block matrices is instead denoted by superscript 'T'. If $\boldsymbol{R}$ and $\boldsymbol{P}$ are second order tensors, we thus have

$$\begin{pmatrix} \boldsymbol{R} \\ \boldsymbol{P} \end{pmatrix}^{\mathsf{T}} = \begin{pmatrix} \boldsymbol{R}, & \boldsymbol{P} \end{pmatrix}, \quad \text{while} \ \begin{pmatrix} \boldsymbol{R} \\ \boldsymbol{P} \end{pmatrix}^{\mathrm{t}} = \begin{pmatrix} \boldsymbol{R}^{\mathrm{t}} \\ \boldsymbol{P}^{\mathrm{t}} \end{pmatrix} \quad \text{and} \quad \begin{pmatrix} \boldsymbol{R} \\ \boldsymbol{P} \end{pmatrix}^{\mathrm{t}\mathsf{T}} = \begin{pmatrix} \boldsymbol{R}^{\mathrm{t}}, & \boldsymbol{P}^{\mathrm{t}} \end{pmatrix}.$$

The 'major' transposition of fourth order tensors is denoted by superscript boldface "$\mathbf{T}$":

$$\mathbf{P}^{\mathbf{T}} = P_{ijk\ell}\, \mathbf{e}_k \otimes \mathbf{e}_\ell \otimes \mathbf{e}_i \otimes \mathbf{e}_j \quad \text{for} \ \mathbf{P} = P_{ijk\ell}\, \mathbf{e}_i \otimes \mathbf{e}_j \otimes \mathbf{e}_k \otimes \mathbf{e}_\ell.$$

The three tensors which, together with the positive scalar field $\rho = \rho(\boldsymbol{x})$, specify the material properties of the micropolar material in **Body** ② residing in $\mathcal{B}$, are the positive definite (second order) moment of inertia tensor $\boldsymbol{J} = \boldsymbol{J}(\boldsymbol{x})$, the (fourth order) elastic stiffness tensor $\mathbf{C} = \mathbf{C}(\boldsymbol{x})$ and the (also fourth order) couple stiffness tensor $\mathbf{D} = \mathbf{D}(\boldsymbol{x})$. The fundamental symmetries of these tensors are

$$\boldsymbol{J}^{\mathrm{t}} = \boldsymbol{J}, \qquad \mathbf{C}^{\mathbf{T}} = \mathbf{C}, \qquad \mathbf{D}^{\mathbf{T}} = \mathbf{D}.$$

The isotropic and homogeneous **Body** ① occupying $\mathcal{B}^\circ$ has the stiffness tensor

$$\mathbf{C}^\circ = \lambda^\circ\, \mathbf{I} \otimes \mathbf{I} + \mu^\circ\, \mathbf{I} \overline{\otimes} \mathbf{I} + \mu^\circ\, \mathbf{I} \underline{\otimes} \mathbf{I} \tag{4}$$

in terms of the Lamé coefficients $\lambda^\circ, \ \mu^\circ$. The couple stiffness tensor $\mathbf{D}$ in **Body** ② residing in $\mathcal{B}$ we take simply to be

$$\mathbf{D} = \alpha\, \mathbf{I} \otimes \mathbf{I} + \gamma\, \mathbf{I} \overline{\otimes} \mathbf{I} + \beta\, \mathbf{I} \underline{\otimes} \mathbf{I} \tag{5}$$

given in terms of the three parameters $\alpha, \ \beta, \ \gamma$. It is thermodynamically admissible for α and β to vanish, for $\gamma > 0$.

Here use is made of the usual outer (tensor) product $\otimes$ as well as of the alternatives $\overline{\otimes}$ and $\underline{\otimes}$. $\overline{\otimes}$ re-arranges the basis vectors, so that

$$\boldsymbol{R} \overline{\otimes} \boldsymbol{S} = R_{ij}\, S_{k\ell}\, \mathbf{e}_i \otimes \mathbf{e}_k \otimes \mathbf{e}_j \otimes \mathbf{e}_\ell \quad \text{for} \ \boldsymbol{R} = R_{ij}\, \mathbf{e}_i \otimes \mathbf{e}_j \ \text{and} \ \boldsymbol{S} = S_{ij}\, \mathbf{e}_i \otimes \mathbf{e}_j,$$

making

$$(\boldsymbol{R} \overline{\otimes} \boldsymbol{S}) \mathbin{:} \boldsymbol{K} = \boldsymbol{R} \bullet \boldsymbol{K} \bullet \boldsymbol{S}^{\mathrm{t}}.$$

$\underline{\otimes}$ re-arranges the basis vectors in another manner:

$$\boldsymbol{R} \underline{\otimes} \boldsymbol{S} = R_{ij}\, S_{k\ell}\, \mathbf{e}_i \otimes \mathbf{e}_\ell \otimes \mathbf{e}_j \otimes \mathbf{e}_k \quad \text{for} \ \boldsymbol{R} = R_{ij}\, \mathbf{e}_i \otimes \mathbf{e}_j \ \text{and} \ \boldsymbol{S} = S_{ij}\, \mathbf{e}_i \otimes \mathbf{e}_j.$$

In addition to being major symmetric, the fourth order tensor $\mathbf{C}^\circ$ is also minor symmetric, *i.e.* in addition to satisfying the major symmetry requirement $\mathbf{C}^{\circ\mathbf{T}} = \mathbf{C}^\circ$, it satisfies

$$\mathbf{C}^\circ = C^\circ_{ijk\ell}\, \mathbf{e}_i \otimes \mathbf{e}_j \otimes \mathbf{e}_k \otimes \mathbf{e}_\ell = C^\circ_{ijk\ell}\, \mathbf{e}_i \otimes \mathbf{e}_j \otimes \mathbf{e}_\ell \otimes \mathbf{e}_k = C^\circ_{ijk\ell}\, \mathbf{e}_j \otimes \mathbf{e}_i \otimes \mathbf{e}_k \otimes \mathbf{e}_\ell.$$

The necessary and sufficient conditions for the internal energy density of **Body** ① to be non-negative are

$$3\lambda^\circ + 2\mu^\circ \geq 0, \quad 2\mu^\circ \geq 0, \qquad \rho^\circ \geq 0. \tag{6}$$

An important point to note is that in order to completely specify the solution of the direct problem, it is necessary to state the boundary conditions also on the *inner* boundaries, *i.e.*, at $\mathcal{P}^\circ$ and at Υ. Without this inner boundary condition, the direct problem of obtaining the displacement (and in the case of **Body** ②, the micro rotation on the outer boundary Γ) from knowledge of $\boldsymbol{g}$ and the material properties in $\mathcal{B}^\circ$ or $\mathcal{B}$, is severely ill posed. If the solution to the direct problem either does not exist or if the existence is non-unique, the point of solving the inverse problem becomes dubious.

2.2. The inner boundary conditions

To be specific, assume that the object to be cloaked inside Υ is a rigid cylindrical body of mass m_c per unit length. If the matter within Γ under any loads on Γ is to respond identically for the cloaked body and the uncloaked line mass, it is necessary that the total mass within the outer boundary is the same in both cases. This is a consequence of Newton's second law in the quasistatic limit. It is well-known and will be discussed in Section 2.3 that the total mass (per unit length) in $\mathcal{B}^\circ$ and in $\mathcal{B}$ are the same. Thus the line mass at $\mathcal{P}^\circ$ in $\mathcal{B}^\circ$ has the same mass as the cloaked cylindrical body, *i.e.* m_c per unit length.

Focusing on the plane strain case discussed above, the line mass at the line $\mathcal{P}^\circ$ in $\mathcal{B}^\circ$ may be regarded as the limit of vanishing radius $r_c \downarrow 0$ of a small massive homogeneous rigid cylindrical body centered at $\mathcal{P}^\circ$. Modify $\mathcal{B}^\circ$ by cutting out the cylindrical body and consider a transformation $\boldsymbol{\psi}$ such the inner boundary cylinder of the modified $\mathcal{B}^\circ$, of radius r_c, is mapped to the inner boundary cylinder Υ of $\mathcal{B}$, of radius r_0. Assume that the transformation at least in some small region close to $r^\circ = r_c$ is a rescaling of the radial distance $r^\circ = |\boldsymbol{x}^\circ - z^\circ \mathbf{e}_z|$ from $\mathcal{P}^\circ$, *i.e.* $\boldsymbol{\psi}(\boldsymbol{x}^\circ) = z^\circ \mathbf{e}_z + (\boldsymbol{x}^\circ - z^\circ \mathbf{e}_z)\psi(r^\circ)/r^\circ$. Here $\mathbf{e}_x$, $\mathbf{e}_y$ and $\mathbf{e}_z$ are fixed coordinates in a Cartesian system established in an inertial frame.

To express the boundary conditions at $r^\circ = r_c$ and $r = r_0$, define

$$\overline{\boldsymbol{r}}^\circ(t) = \overline{x}^\circ(t)\mathbf{e}_x + \overline{y}^\circ(t)\mathbf{e}_y$$
$$\boldsymbol{u}_-^\circ(\varphi^\circ, t) = \overline{\boldsymbol{r}}^\circ(t) + r_c\,\overline{\varphi}^\circ(t)\,\mathbf{e}_{\varphi^\circ}$$
$$\boldsymbol{t}_+^\circ(\varphi^\circ, t) = \boldsymbol{\sigma}_+^\circ(\varphi^\circ, t)\bullet\mathbf{e}_{r^\circ}$$

and

$$\overline{\boldsymbol{r}}(t) = \overline{x}(t)\mathbf{e}_x + \overline{y}(t)\mathbf{e}_y$$
$$\boldsymbol{u}_-(\varphi, t) = \overline{\boldsymbol{r}}(t) + r_0\,\overline{\varphi}(t)\,\mathbf{e}_\varphi$$
$$\boldsymbol{t}_+(\varphi, t) = \boldsymbol{\sigma}_+(\varphi, t)\bullet\mathbf{e}_r.$$

Here $\overline{\boldsymbol{r}}^\circ(t)$ and $\overline{\boldsymbol{r}}(t)$ are the instantaneous positions of the centers of mass of the two massive cylindrical bodies, and $\overline{\varphi}^\circ(t)$, $\overline{\varphi}(t)$ are the angles of rotation of the bodies. $\boldsymbol{u}_-^\circ(\varphi^\circ, t)$ and $\boldsymbol{u}_-(\varphi, t)$ denote the displacements of points on the surfaces of the two bodies, *i.e.* at radius r_c and r_0, respectively. $\boldsymbol{t}_+^\circ(\varphi^\circ, t)$ and $\boldsymbol{t}_+(\varphi, t)$ are the traction vectors in the micropolar materials (for radially outward pointing normals) in the limits $r^\circ \downarrow r_c$ and $r \downarrow r_0$, respectively. Denoting the local force densities exerted on the bounding surfaces of the cylindrical bodies by $\boldsymbol{f}^\circ(\varphi^\circ, t)$ and $\boldsymbol{f}(\varphi, t)$, Newton's 3rd Law implies

$$\boldsymbol{f}^\circ(\varphi^\circ, t) = \boldsymbol{t}_+^\circ(\varphi^\circ, t) \quad \text{and} \quad \boldsymbol{f}(\varphi, t) = \boldsymbol{t}_+(\varphi, t).$$

This, together with Newton's 2nd Law for the rigid cylindrical bodies, yields

$$\int_{-\pi}^{\pi} \boldsymbol{t}_+^\circ(\varphi^\circ, t)\, r_c\, \mathrm{d}\varphi^\circ = m_c\ddot{\overline{\boldsymbol{r}}}^\circ(t) \quad \text{and} \quad \int_{-\pi}^{\pi} \boldsymbol{t}_+(\varphi, t)\, r_0\, \mathrm{d}\varphi = m_c\ddot{\overline{\boldsymbol{r}}}(t).$$

Using the bundle map to relate $\boldsymbol{t}_+^\circ(\varphi^\circ, t)$ to $\boldsymbol{t}_+(\varphi, t)$ then implies that $\ddot{\overline{\boldsymbol{r}}}^\circ(t) = \ddot{\overline{\boldsymbol{r}}}(t)$, so if both start out at rest in their equilibrium positions,

$$\overline{\boldsymbol{r}}^\circ(t) = \overline{\boldsymbol{r}}(t), \quad t \in [0, T].$$

This then holds also in the limit of vanishing r_c.

From the balance of angular momentum for a rigid body we similarly get the relations

$$\int_{-\pi}^{\pi} (r_c\mathbf{e}_{r^\circ}) \times \boldsymbol{t}_+^\circ(\varphi^\circ, t)\, r_c\, \mathrm{d}\varphi^\circ = I_c^\circ\,\ddot{\overline{\varphi}}^\circ(t)\,\mathbf{e}_z \quad \text{and} \quad \int_{-\pi}^{\pi} (r_0\mathbf{e}_r) \times \boldsymbol{t}_+(\varphi, t)\, r_0\, \mathrm{d}\varphi = I_c\,\ddot{\overline{\varphi}}(t)\,\mathbf{e}_z$$

where $I_c^\circ = m_c r_c^2/2$ and $I_c = m_c r_0^2/2$ are the moments of inertia of the cylindrical bodies. Here application of the bundle map implies

$$I_c\,\ddot{\overline{\varphi}}(t) = \frac{r_0}{r_c} I_c^\circ\,\ddot{\overline{\varphi}}^\circ(t), \quad t \in [0, T],$$

i.e., assuming start from rest in equilibrium,

$$\overline{\varphi}(t) = \frac{r_c}{r_0}\,\overline{\varphi}^\circ(t), \quad t \in [0, T].$$

Taking the limit $r_c \downarrow 0$ yields $\overline{\varphi}(t) = 0$, $t \in [0, T]$, provided that $\overline{\varphi}^\circ(t)$ stays bounded in the limit.

Assume that the boundary conditions on Υ are slip boundary conditions, where the tangential part of the traction vanishes, combined with Newton's 2nd and 3rd Laws. The inner boundary condition in Eq. (2e) would then include the following conditions:

$$\mathbf{e}_r \times \boldsymbol{t}_+(\varphi, t) = \mathbf{0} \tag{7}$$
$$\mathbf{e}_r \bullet \boldsymbol{u}_+(\varphi, t) = \mathbf{e}_r \bullet \overline{\boldsymbol{r}}(t) \tag{8}$$
$$\int_{-\pi}^{\pi} \boldsymbol{t}_+(\varphi, t)\, r_0\, \mathrm{d}\varphi = m_c\ddot{\overline{\boldsymbol{r}}}(t), \qquad \overline{\boldsymbol{r}}(0) = \mathbf{0} = \dot{\overline{\boldsymbol{r}}}(0) \tag{9}$$

while Eq. (1e) should include the $r_c \downarrow 0$ limit of the corresponding conditions in the homogeneous domain. And under slip boundary conditions and quiescent initial conditions, both $\overline{\varphi}^\circ(t) = 0$ (which is bounded) and $\overline{\varphi}(t) = 0$ throughout the time interval for $r_c \geq 0$. The inner boundary conditions for the macroscopic fields in Eqs. (1e) and (2e) are thus assumed to be slip boundary conditions, and this ensures that the mappings of the boundary conditions on the macroscopic fields, *i.e.* displacement and traction, at the inner boundary does not cause reflections that impair the cloaking effect.

Note that in the present context a large object is made to behave as if it were an infinitely smaller one of the same mass. Some scattering is then presumed to occur, albeit much less than from an uncloaked large object. It is not unreasonable to consider the objective of the mechanical cloaking to be minimizing the acceleration of the cloaked object, thereby protecting it from incident waves. The ideal case would be if one could achieve $\ddot{\overline{\boldsymbol{r}}}(t) \equiv 0$. And in the limit $r_c \downarrow 0$, this is in fact the case.

To illustrate in a simple case how the rigid body motion vanishes, consider a fixed-frequency scattering problem where the couple parameters α and β vanish, and where the couple stiffness γ goes to infinity. This reduces the transformed problem to the case of a restricted micropolar cloak [17]. Focusing on the boundary conditions at $\mathcal{P}^\circ$ and Υ, assume as above that the body to be cloaked is a homogeneous cylindrical rigid body of mass m_c (per unit length).

We specify the boundary conditions on Υ and at $\mathcal{P}^\circ$ to be the slip conditions described above. As before we consider the line mass to be the limiting case of a small, homogeneous, rigid cylindrical body of radius r_c, as $r_c \downarrow 0$. This is then the limit of a rigid movable scatterer as its radius tends to zero as compared to the wavelengths involved. A somewhat similar case is considered in *e.g.* [23], but the present case exhibits a significant difference.

A useful integral representation of the displacement field is the following:

$$\boldsymbol{u}^{\circ\,\mathrm{inc}}(\boldsymbol{r}^\circ) + \frac{1}{\mu^\circ}\int_{r'=r_c}\left[\boldsymbol{u}^\circ_+(\boldsymbol{r}')\bullet\boldsymbol{\Sigma}^\circ(\boldsymbol{r}',\boldsymbol{r}^\circ) - \boldsymbol{G}^\circ(\boldsymbol{r}',\boldsymbol{r}^\circ)\bullet\boldsymbol{\sigma}^\circ_+(\boldsymbol{r}')\right]\bullet\mathbf{e}_{r'}\, r_c\,\mathrm{d}\varphi' = \begin{cases}\boldsymbol{u}^\circ(\boldsymbol{r}^\circ), & r^\circ > r_c\\ \mathbf{0}, & r^\circ < r_c.\end{cases} \tag{10}$$

(See, *e.g.*, [24], though note a misprint: An erroneous factor of k_S in front of surface integral.) Here $\boldsymbol{u}^{\circ\,\mathrm{inc}}$ is a prescribed incident displacement field, $\boldsymbol{G}^\circ$ is the 2D free-space Green's dyadic, and $\boldsymbol{\Sigma}^\circ$ the 2D free-space Green's stress triadic, with outgoing radiation conditions at infinity. In terms of the basis functions defined above, the incident field may be expanded as

$$\boldsymbol{u}^{\circ\,\mathrm{inc}}(\boldsymbol{r}^\circ) = \sum_{jsm} b_{jsm}\,\boldsymbol{\chi}^{\mathrm{reg}}_{jsm}(r^\circ,\varphi),$$

at least for $r < R$ where R is some radius within which the incident field has no sources. (We consider only $r_c < R$.) Here the partial wave basis functions are

$$\boldsymbol{\chi}^{\mathrm{reg}}_{1sm}(r,\varphi) = \frac{k_P}{k_S}\sqrt{\frac{\pi}{2}}\left[\frac{1}{k_P}\frac{\partial}{\partial r}J_m(k_P r)\boldsymbol{a}_{1sm}(\varphi) + \frac{m}{k_P r}J_m(k_P r)\boldsymbol{a}_{2sm}(\varphi)\right]$$

$$\boldsymbol{\chi}^{\mathrm{reg}}_{2sm}(r,\varphi) = \sqrt{\frac{\pi}{2}}\left[\frac{m}{k_S r}J_m(k_S r)\boldsymbol{a}_{1sm}(\varphi) + \frac{1}{k_S}\frac{\partial}{\partial r}J_m(k_S r)\boldsymbol{a}_{2sm}(\varphi)\right]$$

where the J_m are Bessel functions, and $k_S = \omega\sqrt{\rho^\circ/\mu^\circ}$, $k_P = \omega\sqrt{\rho^\circ/(\lambda^\circ+2\mu^\circ)}$, are the shear and compression wave numbers, respectively. (This is essentially the wave basis in [24].) Furthermore,

$$\boldsymbol{a}_{1sm}(\varphi) = \frac{1}{\sqrt{(1+\delta_{m0})\pi}}\left(\mathbf{e}_x\cos\varphi + \mathbf{e}_y\sin\varphi\right)\left(\delta_{s,\mathrm{even}}\cos m\varphi + \delta_{s,\mathrm{odd}}\sin m\varphi\right)$$

$$\boldsymbol{a}_{2sm}(\varphi) = \frac{1}{\sqrt{(1+\delta_{m0})\pi}}\left(-\mathbf{e}_x\sin\varphi + \mathbf{e}_y\cos\varphi\right)\left(-\delta_{s,\mathrm{even}}\sin m\varphi + \delta_{s,\mathrm{odd}}\cos m\varphi\right).$$

The rigid body motion amplitudes of the cylindrical body of radius r_c may then be explicitly calculated, and approximated for small $k_S r_c$:

$$\begin{aligned}\overline{x}^\circ &= \mathrm{i}\frac{\sqrt{2}\mu^\circ k_S}{N}\left(2b_{2,\mathrm{even},1}\left(k_P r_c H_0^{(1)}(k_P r_c) - 2H_1^{(1)}(k_P r_c)\right)\right.\\ &\quad\left. + b_{1,\mathrm{even},1}\left(2k_S r_c H_0^{(1)}(k_S r_c) + \left(r_c^2 k_S^2 - 4\right)H_1^{(1)}(k_S r_c)\right)\right)\\ &= \left(-\frac{k_S(k_P\, b_{1,\mathrm{even},1} + k_S\, b_{2,\mathrm{even},1})}{\sqrt{2}\,\left(k_P^2+k_S^2\right)\frac{m_c\,\omega^2}{2\pi\,\mu}} + \mathcal{O}[r_c^2]\right)\frac{1}{\ln(k_S r_c)}, \quad \text{when } k_S r_c \ll 1,\end{aligned}$$

$$\begin{aligned}\overline{y}^\circ &= \mathrm{i}\frac{\sqrt{2}\mu^\circ k_S}{N}\left(2b_{2,\mathrm{odd},1}\left(k_P r_c H_0^{(1)}(k_P r_c) - 2H_1^{(1)}(k_P r_c)\right)\right.\\ &\quad\left. + b_{1,\mathrm{odd},1}\left(2k_S r_c H_0^{(1)}(k_S r_c) + \left(r_c^2 k_S^2 - 4\right)H_1^{(1)}(k_S r_c)\right)\right)\\ &= \left(-\frac{k_S(k_P\, b_{1,\mathrm{odd},1} + k_S\, b_{2,\mathrm{odd},1})}{\sqrt{2}\,\left(k_P^2+k_S^2\right)\frac{m_c\,\omega^2}{2\pi\,\mu}} + \mathcal{O}[r_c^2]\right)\frac{1}{\ln(k_S r_c)}, \quad \text{when } k_S r_c \ll 1,\end{aligned}$$

and

$$\overline{\varphi}^\circ = 0.$$

Here $H_m^{(1)}$ is the cylindrical Hankel function of the first kind and order m, and

$$\begin{aligned}N &= H_1^{(1)}(k_P r_c)\left[2k_S H_0^{(1)}(k_S r_c)\left(\pi r_c^2(\lambda^\circ+2\mu^\circ)k_P^2 + \omega^2 m_c\right)\right.\\ &\quad\left. + r_c H_1^{(1)}(k_S r_c)\left(k_S^2\left(\omega^2 m_c - 4\pi\mu^\circ\right) + \pi(\lambda^\circ+2\mu^\circ)k_P^2\left(r_c^2 k_S^2 - 4\right)\right)\right]\\ &\quad + k_P H_0^{(1)}(k_P r_c)\left(H_1^{(1)}(k_S r_c)\left(\omega^2 m_c\left(2 - r_c^2 k_S^2\right) + 2\pi\mu^\circ r_c^2 k_S^2\right) - 2\omega^2 m_c r_c k_S H_0^{(1)}(k_S r_c)\right).\end{aligned}$$

We see that, irrespective of the incident wave, $\overline{\boldsymbol{r}}^{\circ}(t) \equiv \boldsymbol{0}$ in the limit $r_c \downarrow 0$, and since $\overline{\boldsymbol{r}}^{\circ}(t) \equiv \overline{\boldsymbol{r}}(t)$, perfect protection against harmful accelerations can be achieved, at least in theory. Some practical (and computational) difficulties, both for this and the more general case of finite micro stiffness, are dealt with in the numerical section. Note that $\overline{x}^{\circ}$ and $\overline{y}^{\circ}$ converge to zero rather slowly as $k_S r_c \to 0$. (Slower than any positive power of $k_S r_c$.)

It is worth pointing out that for welded boundary conditions, the condition of bounded rigid body rotation is not met, as in this case

$$\begin{aligned}\overline{\varphi}^{\circ} &= \frac{1}{r_c}\frac{4\mathrm{i}\mu^{\circ} b_{2,\mathrm{odd},0}}{\omega^2 m_c r_c H_1^{(1)}(k_S r_c) + 4\pi\mu^{\circ} r_c^2 k_S H_2^{(1)}(k_S r_c)}\\ &= \frac{1}{k_S r_c}\left(-\frac{1}{4+\frac{m_c\omega^2}{2\pi\mu^{\circ}}} + \mathcal{O}[k_S^2 r_c^2]\right) k_S\, b_{2,\mathrm{odd},0}, \quad \text{for } k_S r_c \ll 1.\end{aligned}$$

Welded inner boundary conditions are thus not as suitable for the task of seismic protection. It is perhaps not so surprising that slip conditions are the inner boundary conditions of choice, given the historical precedent set by the ancient greeks, as mentioned in the introduction.

2.3. The cloaking transformation

Here a version of the cloaking transformation discovered by Brun et al. [16] is utilized, in the generalized form given by Norris and Shuvalov [17]. A description is given in this section, and as the general idea behind transformational cloaking is by now rather standard, the description is kept rather brief. One way of describing the cloaking transformation for the present problem is to say that it is a mapping between two vector bundles; one over $\mathcal{B}^{\circ}$, and another over $\mathcal{B}$. The mapping is such that it satisfies what may be called localization of energy, described below, and the special property of the Brun–Norris transformation is that it in addition preserves the scalar character of the mass density. As pointed out already in the very first paper on elastodynamic cloaking [5], and clarified further by Norris and Shuvalov, there are (at least) two components to a cloaking transformation, each more or less independently specifiable. One is the transformation (invertible and differentiable up to some suitable order) between the points of two distinct bodies, a transformation which at the outer boundary reduces to the identity transformation. The second component is the transformation between the displacement fields, which is taken to be a linear transformation that may vary from point to point. So there is a transformation mapping points to points, as well as a what might loosely be called a gauge transformation between vector fields. These components taken together make up the cloaking transformation, which may be regarded as a vector bundle mapping.

To each point $\boldsymbol{x} \in \mathcal{B}$ we thus attach a vector space $V(\boldsymbol{x})$ in which the displacement vector $\boldsymbol{u}(\boldsymbol{x}, t)$ at $\boldsymbol{x}$ lives at any time t, and similarly, for each point $\boldsymbol{x}^{\circ} \in \mathcal{B}^{\circ}$ we have a vector space $V^{\circ}(\boldsymbol{x}^{\circ})$. Define

$$\begin{aligned}\mathcal{V} &= \{((\boldsymbol{x}, t), \boldsymbol{u}) \mid \boldsymbol{x} \in \mathcal{B},\ t \in [0, T],\ \boldsymbol{u} \in V(\boldsymbol{x})\},\\ \mathcal{V}^{\circ} &= \{((\boldsymbol{x}^{\circ}, t), \boldsymbol{u}^{\circ}) \mid \boldsymbol{x}^{\circ} \in \mathcal{B}^{\circ},\ t \in [0, T],\ \boldsymbol{u}^{\circ} \in V(\boldsymbol{x}^{\circ})\}.\end{aligned}$$

$\mathcal{V}$ and $\mathcal{V}^{\circ}$ are vector bundles. The cloaking transformation is the mapping

$$\boldsymbol{\Psi} : \mathcal{V}^{\circ} \longrightarrow \mathcal{V},\ \ ((\boldsymbol{x}^{\circ}, t), \boldsymbol{u}^{\circ}) \mapsto \left((\boldsymbol{\psi}(\boldsymbol{x}^{\circ}), t), \boldsymbol{A}^{\mathrm{t}}(\boldsymbol{x}^{\circ}) \bullet \boldsymbol{u}^{\circ}\right).$$

The two-point, second order, tensor field $\boldsymbol{A}^{\mathrm{t}}(\boldsymbol{x}^{\circ})$, defining a vector field isomorphism at each point $\boldsymbol{x}^{\circ} \in \mathcal{B}^{\circ}$, we assume to be invertible (*i.e*, the matrix formed from its components is non-singular at each point). The vector bundle mapping $\boldsymbol{\Psi}$ is thus a vector bundle isomorphism. Associated with the transformation $\boldsymbol{\psi}$ is the Jacobian two-point tensor of the transformation $\boldsymbol{\psi} = \mathbf{e}_i \psi_i$,

$$\boldsymbol{F} = (\nabla^{\circ} \otimes \boldsymbol{x})^{\mathrm{t}} = \frac{\partial \psi_i(\boldsymbol{x}^{\circ})}{\partial x_j^{\circ}} (\mathbf{e}_i \otimes \mathbf{e}_j),$$

with its Jacobian determinant $\mathrm{J} = \det \boldsymbol{F}$, and its inverse,

$$\boldsymbol{F}^{-1} = (\nabla \otimes \boldsymbol{x}^{\circ})^{\mathrm{t}} = \frac{\partial \psi_i^{-1}(\boldsymbol{x})}{\partial x_j} (\mathbf{e}_i \otimes \mathbf{e}_j),$$

the Jacobian two-point tensor of the inverse transformation $\boldsymbol{\psi}^{-1}$.

Assume that the outer boundary data $\boldsymbol{g}$ is given, and that the inner boundary conditions on $\mathcal{P}^{\circ}$ and Υ have been specified. Introduce the mappings $\boldsymbol{U}_{\boldsymbol{g}}^{\circ}$: $(\boldsymbol{x}^{\circ}, t) \mapsto ((\boldsymbol{x}^{\circ}, t), \boldsymbol{u}^{\circ}(\boldsymbol{x}^{\circ}, t))$ and $\boldsymbol{U}_{\boldsymbol{g}}$: $(\boldsymbol{x}, t) \mapsto ((\boldsymbol{x}, t), \boldsymbol{u}(\boldsymbol{x}, t))$, which map spacetime points in $\mathcal{B}^{\circ} \times [0, T]$ and $\mathcal{B}^{\circ} \times [0, T]$ to points in $\mathcal{V}^{\circ}$ and $\mathcal{V}$, respectively, corresponding to solutions of the respective boundary value problems in Eqs. (1) and (3).

Referring to the diagram in Fig. 3, one may describe part of the task of finding a cloaking transformation as the task of specifying the transformation, together with a vector field isomorphism given by $\boldsymbol{A}^{\mathrm{t}}$ (independent of $\boldsymbol{g}$) such that the diagram commutes for *any* choice of boundary data $\boldsymbol{g}$. (There are of course more requirements to be met by the cloaking transformation; see Fig. 3.)

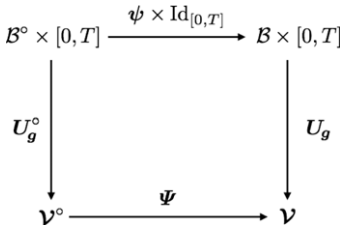

Fig. 3. A diagram over the mappings used in transformational elastodynamic cloaking. To achieve cloaking, the vector field isomorphism should be chosen so that the diagram commutes for any choice of outer boundary data.

Following the approach of Norris and Shuvalov, one may assume *localization of energy*. The kinetic as well as the potential energy density in the two domains, multiplied by their respective volume measures, are then assumed to be locally the same, at corresponding points in $\mathcal{B}^\circ$ and $\mathcal{B}$. The potential energy density in $\mathcal{B}^\circ$ is

$$\mathcal{U}^\circ = \frac{1}{2}\,(\nabla^\circ \otimes \boldsymbol{u}^\circ)^{\mathrm{t}} \vdots \mathbf{C}^\circ \vdots\, (\nabla^\circ \otimes \boldsymbol{u}^\circ)^{\mathrm{t}},$$

and the kinetic energy density is

$$\mathcal{T}^\circ = \frac{1}{2}\rho^\circ\, \dot{\boldsymbol{u}}^\circ \cdot \dot{\boldsymbol{u}}^\circ,$$

where overdot denotes partial derivative with respect to time. If the potential energy density in $\mathcal{B}$ is denoted by $\mathcal{U}$, and the kinetic energy density by $\mathcal{T}$, then

$$\mathcal{U}^\circ \mathrm{d}V^\circ = \mathcal{U}\mathrm{d}V, \quad \text{and} \quad \mathcal{T}^\circ \mathrm{d}V^\circ = \mathcal{T}\mathrm{d}V,$$

where $\mathrm{d}V$ and $\mathrm{d}V^\circ$ are the respective volume elements. Thus

$$\mathcal{U}(\boldsymbol{x},t) = \frac{\mathrm{d}V^\circ}{\mathrm{d}V}\,\mathcal{U}^\circ(\boldsymbol{x}^\circ,t) = \frac{1}{\mathrm{J}(\boldsymbol{x}^\circ)}\,\mathcal{U}^\circ(\boldsymbol{x}^\circ,t), \quad \text{and} \quad \mathcal{T}(\boldsymbol{x},t) = \frac{1}{\mathrm{J}(\boldsymbol{x}^\circ)}\,\mathcal{T}^\circ(\boldsymbol{x}^\circ,t).$$

By means of the mapping $\boldsymbol{\Psi}$, $\mathcal{U}$ may be expressed as

$$\mathcal{U} = \frac{1}{2}\,(\nabla \otimes \boldsymbol{u} + \mathbf{G}\cdot\boldsymbol{u})^{\mathrm{t}} \vdots \mathbf{C} \vdots\, (\nabla \otimes \boldsymbol{u} + \mathbf{G}\cdot\boldsymbol{u})^{\mathrm{t}}. \tag{11}$$

Here

$$\mathbf{G} = (\boldsymbol{F}^{-\mathrm{t}}\overline{\otimes}\boldsymbol{A}^{-\mathrm{t}}) \vdots (\nabla^\circ \otimes \boldsymbol{A}^{\mathrm{t}}),$$

and the stiffness tensor is given by

$$\mathbf{C} = \mathrm{J}\,\mathbf{Q} \vdots \mathbf{C}^\circ \vdots \mathbf{Q}^{\mathsf{T}}, \quad \text{where } \mathbf{Q} = \frac{1}{\mathrm{J}}\boldsymbol{A}\,\overline{\otimes}\,\boldsymbol{F}.$$

We want the expression for $\mathcal{U}$ in Eq. (11), derived through the transformation $\boldsymbol{\Psi}$, to be identical to the one derived from the solution to the equation of motion in the inhomogeneous restricted micropolar solid.

A basic requirement of elastodynamics is objectivity, *i.e.*, frame independence. The presence of $\mathbf{G}\cdot\boldsymbol{u}$ inthe transformed potential energy density in Eq. (11) makes the energy expression non-objective. $\mathbf{G}$ acts essentially like a connection, and its presence implies that the material would behave as if elastic springs linked the material to an absolute undeformed position. However, for the present case we use the vector field isomorphism given by $\boldsymbol{A}^{\mathrm{t}} = \mathbf{I}$, so $\mathbf{G} \equiv \mathbf{0}$. This vector field isomorphism also ensures that the transformed mass density is scalar, as

$$\rho = \frac{1}{\mathrm{J}}\rho^\circ. \tag{12}$$

From Eq. (12), a property sometimes called preservation of cloaking space, is obvious: The total mass of the cloaking material in $\mathcal{B}$, and the total mass of the homogeneous material in $\mathcal{B}^\circ$ are the same. Since the diffeomorphic transformation between points in $\mathcal{B}$ and $\mathcal{B}^\circ$ may be chosen in many ways, one may in particular specify it to be such that the mass density is constant throughout the cloak. The density then scales with the total volumes of in $\mathcal{B}$ and $\mathcal{B}^\circ$. One such transformation is utilized in the present paper.

Having found a specification for the potential energy density and the kinetic energy density for $\mathcal{B}$, the equation of motion is the Euler–Lagrange equation for the Lagrange density $\mathcal{L} = \mathcal{U} - \mathcal{T}$:

$$\frac{\partial \mathcal{L}}{\partial \boldsymbol{u}} - \nabla\cdot\frac{\partial \mathcal{L}}{\partial(\nabla\otimes\boldsymbol{u})^{\mathrm{t}}} - \frac{\partial}{\partial t}\frac{\partial \mathcal{L}}{\partial \dot{\boldsymbol{u}}} = 0.$$

The constitutive relation giving the stress $\boldsymbol{\sigma}$ may be obtained from the strain energy density as

$$\boldsymbol{\sigma} = \frac{\partial\, \mathcal{U}}{\partial(\nabla \otimes \boldsymbol{u})^{\mathrm{t}}} = \mathbf{C} \vdots (\nabla \otimes \boldsymbol{u})^{\mathrm{t}}.$$

There is no *a priory* guarantee that the equation of motion and the constitutive relation so obtained really correspond to any physically realizable material. However, it does correspond exactly to the restricted micropolar material with the choices of stiffness and density indicated. The reason for including also the unrestricted micropolar material in our discussion is in fact that the physical properties of the restricted micropolar medium are unrealistic. This point may be described in the following manner: Consider the micro rotation field in an unrestricted micropolar medium. From the mechanics of the assumed microstructure, one would expect that

$$\boldsymbol{\phi}(\boldsymbol{x}, t) = \mathcal{O}\left[\|\boldsymbol{\jmath}\|^{-\zeta_0}\right]\left(\boldsymbol{\phi}_0(t) + \mathcal{O}\left[\|\mathbf{D}\|^{-\zeta_1}\right]\boldsymbol{\phi}_1(\boldsymbol{x}, t)\right), \quad \text{as } \|\boldsymbol{\jmath}\| \to \infty \text{ and/or } \|\mathbf{D}\| \to \infty. \tag{13}$$

(Here the ζ_i are positive exponents. For simplicity we assume that all elements of the inertia tensor are to grow proportionally, and similarly for the stiffness tensor.) As the elements of the moment of inertia of the microscale bodies go to infinity, $\boldsymbol{\phi}(\boldsymbol{x}, t)$ vanishes, while if the micro stiffnesses go to infinity, all we may expect is to get a micro rotation field that is constant in space. But the elements of the moment of inertia tensor of the microscale bodies are bounded by some multiple of the (local average) density and the square of the linear size of the representative volume element, containing the microscale body. In practice it may thus not be physically realistic to expect $\boldsymbol{\jmath}$ to be so large that $\boldsymbol{\phi}(\boldsymbol{x}, t)$ effectively vanishes.

Even if the couple stiffness could be made arbitrarily large, Eq. (13) is in fact oversimplified, due to a complication brought on by possible resonances. For fixed moment of inertia and increasing couple stiffness, a (in theory infinite) number of resonances are encountered. So while the *infimum limit* of the micro rotation may be zero, as the couple stiffness goes to infinity, there is no reason to believe that the *limit* of the micro rotation is zero. A pertinent question is then as to what extent an unrestricted micropolar cloak may be used as an effective approximation of the restricted micropolar cloak. This is a question to be explored numerically.

2.4. The outer boundary conditions

In the discussion above, we have formulated everything as a boundary value problem, where the traction is specified on the outer boundary Γ. This formulation is useful for discussing the traction-to-displacement maps of the various bodies. As the focus here is on the scattering properties of the bodies, let us instead consider the bodies in $\mathcal{B}^\circ$ and $\mathcal{B}$ to be embedded in a homogeneous and isotropic solid, with the properties of the material of the homogeneous reference body, **Body** ③. To ensure continuity of the displacement field across Γ, it is required that $\boldsymbol{A}^{\mathrm{t}} \to \mathbf{I}$ as $\boldsymbol{x}$ approaches Γ from the inside. But in the present case of the generalized Brun transformation, this is trivially so, since $\boldsymbol{A}^{\mathrm{t}} \equiv \mathbf{I}$.

The transformation $\boldsymbol{\psi}$ is assumed to approach the identity transformation at the outer boundary, but the Jacobian tensor $\boldsymbol{F}$ need in fact not approach $\mathbf{I}$. (Unless of course the vector field isomorphism is chosen so as to force the Jacobian tensor to inherit the requirement $\boldsymbol{A}^{\mathrm{t}} \to \mathbf{I}$, *e.g.*, if $\boldsymbol{A} = \boldsymbol{F}$, as for Willis type materials.) This was discovered by Brun et al. for a special case [25], but is quite general. There may thus be a mismatch both in the stiffness tensor and in the deformation gradient across the outer boundary of $\mathcal{B}$, and still the continuity of both traction and displacement may hold across the boundary. That this is true, not only in the special case considered by Brun et al., is seen from the fact that on Γ, for *any* vector field isomorphism $\boldsymbol{A}^{\mathrm{t}}$,

$$(\mathbf{C} \vdots (\nabla \otimes \boldsymbol{u} + \mathbf{G} \bullet \boldsymbol{u})^{\mathrm{t}}) \bullet \boldsymbol{n} = (\mathbf{C}^\circ \vdots (\nabla^\circ \otimes \boldsymbol{u}^\circ)^{\mathrm{t}}) \bullet \boldsymbol{n}$$

irrespective of whether $\boldsymbol{F}$ approaches $\mathbf{I}$. For such vector field isomorphisms $\boldsymbol{A}^{\mathrm{t}}$ that make $\mathbf{G} \bullet \boldsymbol{u}$ vanish, we then have

$$\mathbf{G} \bullet \boldsymbol{u} \equiv \mathbf{0} \Rightarrow \sigma \bullet \boldsymbol{n} = (\mathbf{C} \vdots (\nabla \otimes \boldsymbol{u})^{\mathrm{t}}) \bullet \boldsymbol{n} = (\mathbf{C}^\circ \vdots (\nabla^\circ \otimes \boldsymbol{u}^\circ)^{\mathrm{t}}) \bullet \boldsymbol{n} = \boldsymbol{\sigma}^\circ \bullet \boldsymbol{n}. \tag{14}$$

To satisfy requirements of continuity of displacement and traction over the outer boundary of the cloak, the second component of the vector bundle mapping need thus only approach $\mathbf{I}$ in C^0 as $\boldsymbol{x} \to \Gamma$.

3. Numerical simulation

The unrestricted micropolar (imperfect) cloak is arguably more realistic than the restricted micropolar (perfect) cloak. The latter requires a quantity, the moment of inertia density, to take infinite or at least unrealistically large values. As mentioned above, the moment of inertia density is bounded by the product of some multiple of the density and the square of the linear size of the microstructural unit cell.

To model both the restricted and the unrestricted micropolar medium, a commercial software, COMSOL Multiphysics™ is used. We may note that COMSOL Multiphysics™ only has a fully symmetric (both minor and major symmetric) elasticity tensor implemented into the software, presumably reflecting the fact that a majority of 'commercially interesting FE problems only require symmetric elasticity. The minor asymmetry required here can be implemented through some modification in the Structural Mechanics module of COMSOL Multiphysics™. However, instead developing a model within the PDE

module is more straightforward, and simplifies the switch between the classical Cauchy type continuum and the micropolar continuum in the following studies. (To validate the implementation, the results from Brun et al. [16,25] were reproduced.)

The slip boundary conditions on the inner boundary of the cloaking layer (*cf*. Section 2.2) may be implemented in various ways. Using the built in "Roller" boundary condition in COMSOL proved to be problematic in the current version (v4.3), instead a very thin elastic layer is inserted between the rigid body and the cloak. The layer has a high stiffness in the normal direction but essentially vanishing stiffness in the tangential direction. The boundary condition of vanishing micro moment vector (as discussed in Section 2.4) at the outer and inner boundaries of the cloak, is enforced in a weak sense in the PDE module.

3.1. Coordinate transformation in 2D—dealing with infinities

As discussed in Section 2.2, when the radius of the inverse map of the cloaked rigid body vanishes, the mass center of the body becomes immovable. As shown in Fig. 4, this decay to zero is apparent both for Rayleigh waves in the surface-breaking (Fig. 4(a)) and the sub-surface (Fig. 4(b)) cases, as well as for a bulk wave in the free-space case (Fig. 4(c)). The rate of decay to zero mobility in Fig. 4(c), is seen to agree well with the analytical results of Section 2.2. In addition, a resonance effect, to be discussed below, for certain combinations of stiffness and density, is suggested in the figures. The "rigid" cylinder is modeled as an elastic cylinder with a factor of 1000 times higher stiffness compared to the surrounding material in all of the numerical calculations, compare this to the situation where a cylinder made of steel is embedded in clay soil.

When the rigid body is mapped to a point or line under the inverse transformation, *cf*. the upper part of Fig. 5, diverging stiffnesses and densities in the vicinity of the inner boundary of the cloak are clearly an unphysical feature. A partial cloak can still be achieved using a coordinate transformation taken from a small but finite sized cylinder into the cloak region, see the bottom part of Fig. 5. In this way, the material parameters remain finite. The cost for this is that the acceleration of the center of mass of the partially cloaked rigid body increases as a function of the radius of the reference cylinder, in addition to the increased scattering due to imperfect cloaking.

Another, related, effect to consider is the connection between the size of the microstructural elements, the mesh size of the finite element model, and the 'degree of perfection' of the cloak: To fully resolve the fields around the circumference of a line mass or point mass, the surrounding local mesh element size would have to be infinitely small. However, in the cloaking region we have no reason to consider much smaller mesh sizes than the size determined by the cells of the actual microstructure. The sizes of the cloak mesh elements, when mapped back to the neighborhood of the reference cylinder, can only yield a limited resolution of the radius r_c. Thus the 'degree of perfection' of the cloak is to an important part determined by the size of the microstructural elements in the neighborhood of the rigid body.

3.2. Parametric study of the material properties inside the unrestricted micropolar cloak

As discussed in Section 2.3, the restricted micropolar cloak should, if resonances did not complicate matters, correspond to an infinite moment of inertia, see Eq. (13). However, the moment of inertia is bounded by (a product of) the density and the squared linear dimension of the microstructural units. Given the bound on the moment of inertia, letting the couple stiffness grow, should at most lead to a micro rotation that is constant in space throughout the cloak.

In Fig. 6 we consider the influence of these parameters. Fig. 6(a) indicates that the micro rotation for fixed moment of inertia does tend to a constant value for high couple stiffnesses. Fig. 6(b) illustrates the point that, while the infimum limit of the micro rotation is zero for fixed couple stiffness as the moment of inertia increases, the resonances prevents any actual limit to be obtained.

The rightmost tail of the curve in Fig. 6(b) may lead you to believe that the resonances disappear for the highest values of the moment of inertia. However, the absence of resonances in the tail is due to the fact that the finite dimensional FE representation can at most resolve a finite number of resonances. Increasing the number of elements, we find that more resonances appear. Fig. 7 shows how some of the resonances appear in parameter space as sharp mountain ridges. A finer mesh would here result in more eigenvalues being resolved in the computation and thus in an increased number of resonance ridges.

3.3. Numerical results

Consider two cases of buried elastic cylinders impinged upon by an elastic surface wave. One case is a cylinder that is buried completely, but still close to a free surface. The other case is an only half buried, surface breaking, cylinder. The cylinders are modeled as elastic with a factor of 1000 times higher stiffness compared to the surrounding material, compare this to the situation where a cylinder made of steel is embedded in clay soil. The incident wave is a Rayleigh wave, and thus consists of a combination of vertically attenuated plane compression and shear waves. In order to compare the effectiveness of a (physically much harder to construct) restricted micropolar cloak to that of an unrestricted micropolar cloak, we compute the acceleration of the center of mass of the cylinders in the time domain. The resulting orbits are shown in Fig. 8, where also the accelerations for uncloaked cylinders are shown. To avoid problems with unphysical densities (vanishing or infinite) in the cloaking materials, we chose the transformation such that the mass densities within the cloak are constant throughout the cloaks.

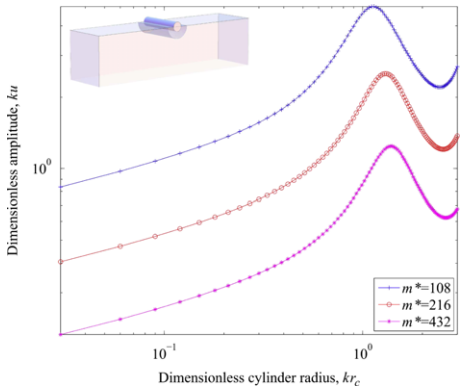

(a) Displacement response of a surface breaking cylinder to an incident Rayleigh wave as $r_c \to 0$.

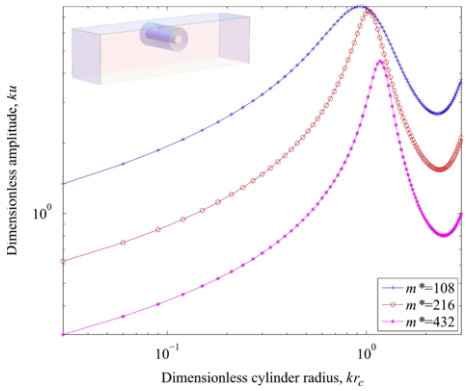

(b) Displacement response of a sub-surface cylinder to an incident Rayleigh wave as $r_c \to 0$.

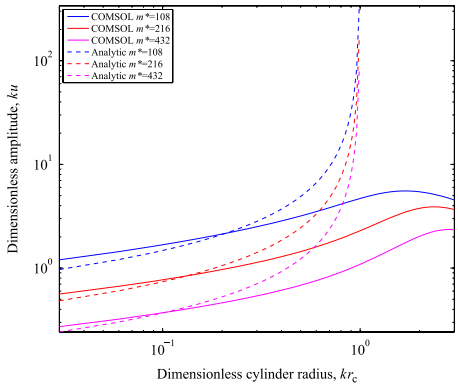

(c) Displacement response of a cylinder (in a full space) to an incident P wave as $r_c \to 0$. Comparison of numerical solution to asymptotic solution.

Fig. 4. The dimensionless mass is $m^* = mk^3/\rho$, where m is the mass of the rigid-body, $k = k_S$ is the wavenumber for an S wave, ρ is density of the homogeneous medium, u the displacement of the rigid-body and r_c is the radius of the rigid-body. The reason that the curves diverge in the right half of the plot is the fact that only the lowest terms in the analytical expression have been plotted.

As can be seen in both cases in Fig. 8, the restricted micropolar cloak is, as expected, effective in protecting the object from the incident wave. The unrestricted micropolar cloak does indeed for (low moment of inertia and) high couple stiffness well mimic the restricted cloak, showing that the physically more realistic unrestricted micropolar cloak may be used to protect objects against potentially harmful, surface wave induced accelerations. The effectiveness may easily be increased by reducing the parameter r_c (the radius of the 'abstract' inverse image of the cloaked cylindrical body). In practice this would, as discussed in Section 3.1, demand decreasing the size of the microstructural elements.

In Fig. 8 there are also included worst and best cases obtained by considering also smaller couple stiffnesses. It would be tempting to try to achieve in particular the very low accelerations that are possible by placing the stiffness very close to a resonance value. However, this involves a parametrical balancing act, as a slight change in frequency or some other parameter might flip a small acceleration into a very large one.

In Fig. 9 we see a snapshot of the wave field when steady state conditions have been established, both for an uncloaked and for a cloaked surface breaking rigid cylinder. As indicated above, the cloak is an unrestricted micropolar one, with a constant mass density. It is clear in the figure that the reflection from the cylinder is far smaller in the cloaked case, as the wave mostly passes beneath it. And the acceleration of the cylinder is, as we have already seen, significantly less in the cloaked case: As the wave field is only slightly affected by the cylinder, the cylinder is only slightly affected by the wave field. For the sub-surface cylinder, the same effect is apparent in Fig. 10.

4. Concluding remarks

In this paper, we have discussed the possibilities for cloaking of structures using transformational elastodynamics. The procedure can be summarized in three steps: (i) the ansatz of a topology (dimension) in a fictitious domain that would result in a required response (Body ①), (ii) the design of a restricted micropolar continuum surrounding the structure to be cloaked that identically mimics the response of the former (Body ③), and (iii) the relaxation of the restricted micropolar continuum

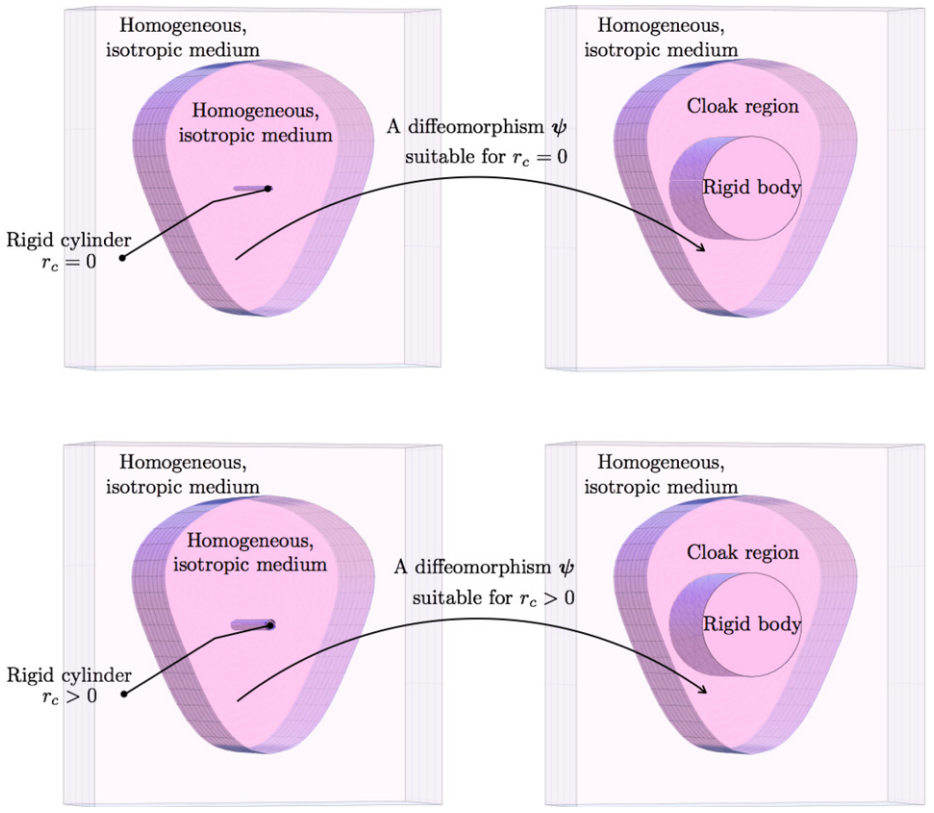

Fig. 5. A schematic representation of the cloaking transformation. The upper part illustrates the transformation taken from a point, $r_c = 0$ and the bottom part illustrates the transformation taken from a finite cylinder, $r_c \neq 0$.

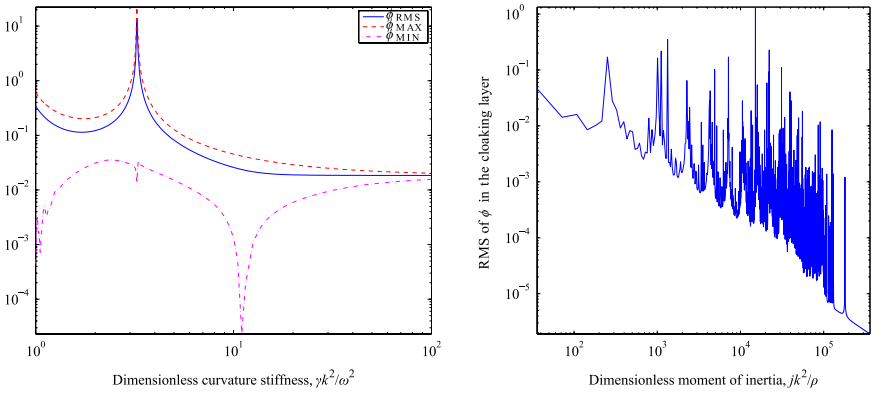

(a) Increasing couple stiffness, constant moment of inertia.

(b) Increasing moment of inertia, constant couple stiffness.

Fig. 6. Parametric study of the couple stiffness and the moment of inertia density in the cloaking layer. Here γ is the couple stiffness of the cloaking layer, j is the moment of inertia density of the cloaking layer, $k = k_S$ is the wavenumber for an S wave, ρ is the mass density of the homogeneous medium and ω is the angular frequency.

to an unrestricted counterpart (Body ②) that corresponds to a physically realizable material. The feasibility of the approach has been investigated for subsurface and surface-breaking two dimensional structures subjected to Rayleigh waves.

An almost perfect cloak is obtained upon letting the size of the structure tend to zero in the fictitious domain (the deviation from perfect cloaking is due to the non-vanishing, albeit small, scattering from the point-mass). Numerical as well as analytical solutions for a cylinder in 2d have been investigated. The relation between the finite element discretization of a perfect cloak and the exact solution to a problem with finite dimension structure ($r_c > 0$) has been identified. In practice, the lower limit of the dimension in the fictitious domain is governed by the material data one is able to physically realize.

The relaxation of the theoretical restricted micropolar material to a physically sound unrestricted micropolar material has been investigated numerically. One may conclude that the limit of high couple stiffness together with high moment of inertia

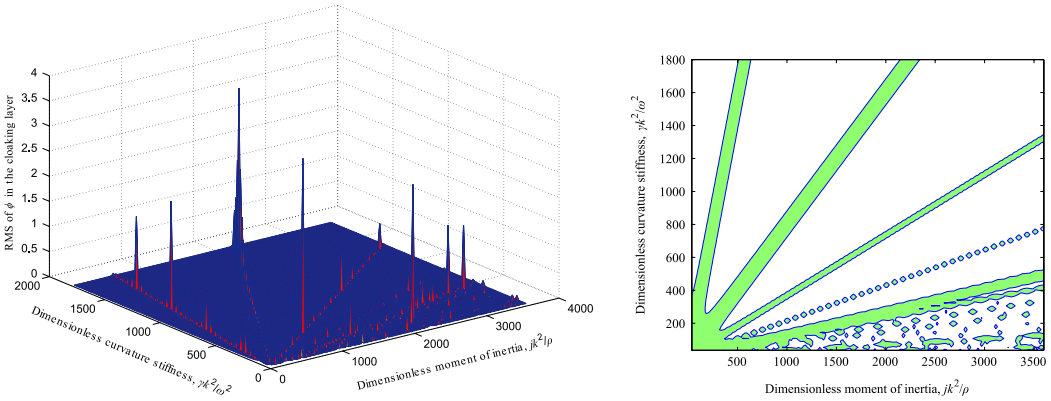

(a) Surface plot showing resonances.

(b) Contour plot showing resonances.

Fig. 7. Parametric study of different combinations of the couple stiffness and the moment of inertia density. Here γ is the couple stiffness of the cloaking layer, j is the moment of inertia density of the cloaking layer, $k = k_S$ is the wavenumber for an S wave, ρ is the mass density of the homogeneous medium and ω is the angular frequency.

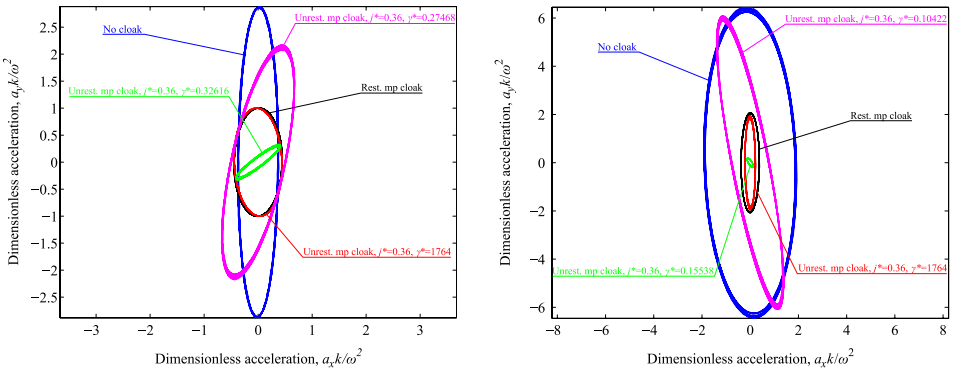

(a) Acceleration of a surface breaking cylinder.

(b) Acceleration of a sub-surface cylinder.

Fig. 8. Acceleration comparison of a cylinder subjected to Rayleigh waves after long time. Here a is the acceleration of the cylinder, $k = k_S$ is the wavenumber for an S wave, ω is the angular frequency, γ is the couple stiffness of the cloaking layer and j is the moment of inertia density of the cloaking layer.

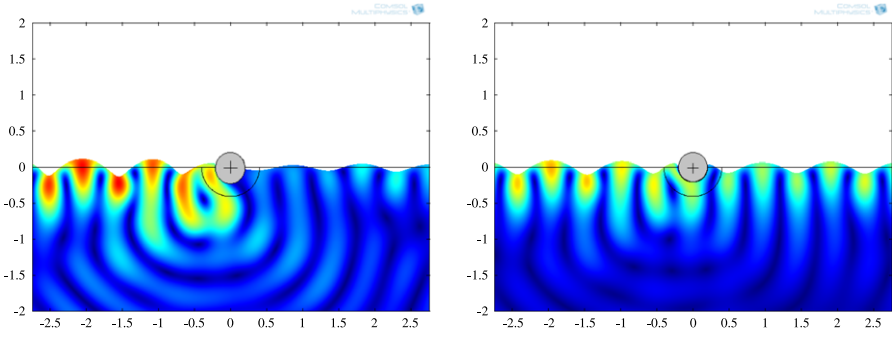

(a) Uncloaked configuration, surface breaking cylinder.

(b) Cloaked configuration, surface breaking cylinder.

Fig. 9. Results from COMSOL Multiphysics™ as displacement surface plots, comparing the uncloaked and the cloaked configuration. In (a) the region between the outer and the inner semi-circles contains the same homogeneous and isotropic material as the surrounding sub-surface material. In (b) the same region contains a graded unrestricted micropolar cloak.

results in a material approaching that of restricted micropolar. However, the moment of inertia is in practice bounded by the density and the geometrical size of the microstructure, and can thus not be controlled arbitrarily. For varying the couple stiffness, it is identified that the highest possible value guarantees the best cloak. For a given frequency, however, lower couple stiffness can result in an even better cloak.

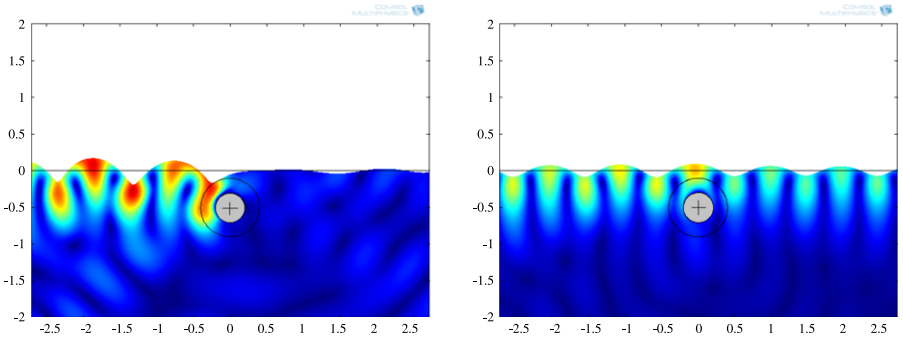

(a) Uncloaked configuration, sub-surface cylinder. (b) Cloaked configuration, sub-surface cylinder.

Fig. 10. Comparison between the uncloaked and the cloaked configuration, for a Rayleigh wave impinging on a sub-surface rigid cylinder. In (a) the region between the outer and the inner circles contains the same homogeneous and isotropic material as the surrounding sub-surface material. In (b) the same region contains a graded unrestricted micropolar cloak.

The possibility to cloak a cylinder in 2D has thus been shown, limited only by the coefficients in an unrestricted micropolar media. In order to realize a cloaking procedure in practice, future work will concern the actual design of a microstructure exhibiting the required micropolar properties investigated in this paper.

Acknowledgments

This research was supported by the Swedish Research Council Grants No. 621-2012-3134. Special thanks to Senad Razanica for all of his assistance during the investigation in COMSOL Multiphysics™.

References

[1] Pliny the Elder, Pliny's Natural History, Volume X: Book 36, XXI, Harvard University Press, Massachusetts, 1954, (Translated by D. E. Eichholz).
[2] S. Brûlé, H. Javelaud, E.S. Enoch, S. Guenneau, Experiments on seismic metamaterials: Molding surface waves, Phys. Rev. Lett. 112 (2014) 133901.
[3] A. Greenleaf, M. Lassas, G. Uhlmann, On nonuniqueness for Calderon's inverse problem, Math. Res. Lett. 10 (2003) 685–693.
[4] J.B. Pendry, D. Schurig, D.R. Smith, Controlling electromagnetic fields, Science 312 (2006) 1780–1782.
[5] G.W. Milton, M. Briane, J.R. Willis, On cloaking for elasticity and physical equations with a transformation invariant form, New J. Phys. 8 (2006) 1–21.
[6] A.N. Norris, Acoustic cloaking theory, Proc. R. Soc. A: Math. Phys. Eng. Sci. 464 (2008) 2411–2434.
[7] F.G. Vasquez, G.W. Milton, D. Onofrei, P. Seppecher, Transformational elastodynamics and active exterior acoustic cloaking, in: Acoustic Metamaterials, in: Springer Series in Materials Science, vol. 166, 2013, pp. 289–318.
[8] A. Norris, F. Amirkulova, W. Parnell, Active elastodynamic cloaking, Math. Mech. Solids 19 (2014) 603–625.
[9] A. Norris, W. Parnell, Hyperelastic cloaking theory: Transformation elasticity with pre-stressed solids, Proc. R. Soc. A 468 (2012) 2881–2903.
[10] W. Parnell, A. Norris, T. Shearer, Employing pre-stress to generate finite cloaks for antiplane elastic waves, Appl. Phys. Lett. 100 (2012) 171907.
[11] W. Parnell, Nonlinear pre-stress for cloaking from antiplane elastic waves, Proc. R. Soc. A 468 (2012) 563–580.
[12] J. Hu, Z. Chang, G. Hu, Approximate method for controlling solid elastic waves by transformation media, Phys. Rev. B 84 (2011).
[13] M. Farhat, S. Guenneau, S. Enoch, Ultrabroadband elastic cloaking in thin plates, Phys. Rev. Lett. 103 (2009) 024301.
[14] M. Brun, D. Colquitt, I. Jones, A. Movchan, N. Movchan, Transformational cloaking and radial approximations for flexural waves in elastic plates, New J. Phys. 16 (2014) 093020.
[15] D. Colquitt, M. Brun, M. Gei, A. Movchan, N. Movchan, Transformation elastodynamics and cloaking for flexural waves, J. Mech. Phys. Solids 72 (2015) 131–143.
[16] M. Brun, S. Guenneau, A.B. Movchan, Achieving control of in-plane elastic waves, Appl. Phys. Lett. 94 (2009) 1–3.
[17] A.N. Norris, A.L. Shuvalov, Elastic cloaking theory, Wave Motion 48 (2011) 525–538.
[18] A. Eringen, Linear theory of micropolar elasticity, J. Math. Mech. 15 (6) (1966) 909–923.
[19] V.A. Eremeyev, L.P. Lebedev, H. Altenbach, Foundations of Micropolar Mechanics, in: SpringerBriefs in Applied Sciences and Technology, 2013, pp. 35–66.
[20] P. Olsson, D.J.N. Wall, Partial elastodynamic cloaking by means of fiber-reinforced composites, Inverse Problems 27 (2011) 045010.
[21] R. Kohn, H. Shen, M. Vogelius, M. Weinstein, Cloaking via change of variables in electric impedance tomography, Inverse Problems 24 (2008) 015016.
[22] D. Colquitt, I. Jones, N. Movchan, A. Movchan, M. Brun, R. McPhedran, Making waves round a structured cloak: lattices, negative refraction and fringes, Proc. R. Soc. A 469 (2013).
[23] P. Olsson, The rigid movable inclusion in elastostatics and elastodynamics, Wave Motion 7 (1985) 421–445.
[24] A. Karlsson, Scattering of rayleigh lamb waves from a 2D-cavity in an elastic plate, Wave Motion 6 (1984) 205–222.
[25] M. Brun, S. Guenneau, A.B. Movchan, Invisibility to in-plane elastic waves, in: XIX Congresso AIMETA, Ancona, Italy, 14–17 September, 2009.